Study on Accurate Grading Prediction Model of Tobacco Weather Fleck Based on Internet of Things

Jiazhao Sun
Southwest University
Xiaoli Hao
Guizhou Minzu University
Yuao Ran
Southwest University
GOH MARK
NUS Business School, National University of Singapore
Zhenguo Wang
China National Tobacco Corporation Fengjie Branch
Yabo Jin
China Tobacco Guangxi Industry Corporation Limited
Wei Ding
dingw@swu.edu.cn
Southwest University

Article

Keywords: Accurate prediction, Field Internet of Things (IoT), Hierarchical identification, Significance factors, Tobacco weather fleck

Posted Date: April 15th, 2025

DOI: https://doi.org/10.21203/rs.3.rs-6175007/v1

Additional Declarations: No competing interests reported.

Study on Accurate Grading Prediction Model of Tobacco Weather Fleck Based on Internet of Things

Jiazhao Sun[1], Xiaoli Hao[2], Yuao Ran[1], GOH MARK[3], Zhenguo Wang[4], Yabo Jin[5,*] & Wei Ding[1,*]

[1]Laboratory of Natural Products Pesticides, College of Plant Protection, Southwest University, Chongqing 400715, China.

[2]School of Sociology, Guizhou Minzu University, Guiyang 550025, China.

[3]NUS Business School and The Logistics Institute - Asia Pacific, National University of Singapore, 699010, Singapore.

[4]China National Tobacco Corporation Fengjie Branch, Chongqing 400715, China.

[5]China Tobacco Guangxi Industry Corporation Limited, Nanning 530001, China.

*****Email: dingw@swu.edu.cn;338390768@qq.com.

Abstract: Precise prediction of crop disease trends and accurate grading identification of diseases based on information technology represent a significant challenge in the application of IoT devices in agricultural production. Addressing this issue necessitates the development of predictive models for the efficient representation of Internet of Things (IoT) data. In this context, a graded precision forecasting model for Tobacco weather fleck has been developed. Additionally, a graded recognition model has been constructed to identify different levels of disease severity based on the aforementioned grading system. We utilized meteorological data collected from field Internet of Things (IoT) devices and employed the Generalized Additive Model (GAM) to identify factors significantly associated with the occurrence of this disease. The proposed composite model, which leverages the search capability of the Grey Wolf Optimizer (GWO) and the feature extraction advantage of Convolutional Neural Networks (CNN), optimized the Long Short-Term Memory (LSTM) model (GWO-CNN-LSTM) for the best grading prediction effect of tobacco climate spot disease (accuracy rate of 85.46%). The GoogleNet model, optimized with the Convolutional Block Attention Module (CBAM) and based on the Inception-ResNet-v2, achieved the highest accuracy rate for disease grading recognition (92.40%), which was significantly higher than the manual recognition accuracy rate (83.00%; P<0.05). The experimental results demonstrate the precise prediction and identification of varying degrees of tobacco climate spot disease occurrence. The proposed model makes a positive contribution to the knowledge system of crop disease grading prediction and the advancement of Internet of Things (IoT) agriculture.

Keywords Accurate prediction, Field Internet of Things (IoT), Hierarchical identification, Significance factors, Tobacco weather fleck

The global food system is currently under pressure due to rising population, economic growth, land degradation, and increased demand for plantation-based products[1]. Precision agriculture can increase the resilience of agricultural systems to adapt to the challenges posed by diverse change, thereby guaranteeing global food security[2]. The Internet of Things (IoT), an important part of precision agriculture, opens up new opportunities for monitoring agricultural and food processing processes[3]. The technology can capture data from agricultural production through front-end sensors and deliver it to computing devices in real time, which provides a prerequisite for the development and application of large agricultural models[4]. Driven by Internet (IoT) technology, the use of agricultural models in crop monitoring, the application of IoT offers many new opportunities for farmers to optimize crop production and resource utilization. Machine learning (e.g., artificial neural network models) has been used for crop growth condition prediction to automate and accurately apply water, fertilizers, herbicides, and pesticides[5]. The aim of this practice is to reduce costly inputs, crop losses, and environmental impacts caused by improper use of drugs and fertilizers, while improving economic efficiency.

Each year, 20%–40% of crops are lost due to plant pests and pathogens[6]. Worldwide, yield losses caused by pests and diseases are estimated to average 21.5% in wheat, 30.0% in rice, 22.6% in maize, 17.2% in potato, and 21.4% in soybean[7]. With plant unhealthiness causing such serious crop problems, focusing on the implementation of plant protection using IoT in combination with precision agriculture technology is a key research priority. A study uses machine learning to model crop water requirements under different climatic conditions, to address unhealthy crop water loss and to improve water use[8]. Beyond the issue of crop water use, the impact of changing climatic conditions on crops has been shown more often to be in the form of diseases suffered during crop growth[9]. The implementation of intelligent crop disease prediction systems at the agricultural production level can help reduce crop losses as well as support farmers and managers in making the right decisions.

Computer-developed agricultural-related models play an important role as the “brain” of the disease prediction system. Liu et al.[10] applied the Internet of Things (IoT) to sense the meteorological conditions of farmland and used a machine learning approach for early prediction of the probability of blister blight attack in tea trees. Singh et al.[11] employed the results of different machine learning methods for comparison to predict the epidemiological characteristics of mustard white rust and explained the role of weather variables in the prediction. Among many machine learning models, long short-term memory (LSTM) network is widely used in crop disease prediction model construction. Lu et al.[12] extracting serialized features from IoT data using Long Short-Term Memory (LSTM) networks. Construction of a multimodal data fusion-based prediction model for lychee frosty blight using sensitive characterization factors closely related to lychee frosty blight disease, with an accuracy of 89.58%. Kim et al.[13] studied four indicators to build Rice Blast prediction model using (LSTM) model for early occurrence prediction of rice blast in the field. Krishna et al.[14] applied an optimized LSTM model to fit climate parameters to model the incidence of fruit rot in betel nut crops, which helps farmers to reduce unnecessary fungicide applications and obtain more favorable yields. The Long Short-Term Memory (LSTM) model is able to learn long-term dependencies due to its ability to control the flow of information through a special gating mechanism. The gradient vanishing problem is mitigated thus allowing deeper networks to be trained. As well as its flexibility to be easily combined with other types of neural network structures, it is rapidly emerging as an efficient solution in deep learning modeling[15-17]. Therefore, the prediction model of crop diseases can be established by using the Long Short-Term Memory (LSTM) network or the optimized and improved network model based on it in combination with the IoT technology.

Tobacco, as a multi-attribute commodity, has a high economic value, and in some regions tobacco farming is considered the backbone of the economy[18,19]. During tobacco cultivation, leaf diseases have been the cause of great losses in crop growth, resulting in reduced tobacco yields and quality. Tobacco weather fleck is one of the major foliar diseases of tobacco that occurs during field growth and is non-invasive. An imbalance in atmospheric ozone concentrations as a result of climate change has been widely documented as a trigger for the disease[20,21]. Although chemical control (pesticide spraying) and physical control (drainage and ventilation of field ridges) are used to control the disease, the cost of pesticides has increased, and environmental pollution caused by pesticide residues threatens the health of cultivation Therefore solutions are needed, with the help of IoT, weather, models can accurately predict the occurrence of disease before it damages the plants in order to effectively control the onset of disease to reduce environmental pollution.

Regarding image recognition, currently the main focus is on symptom recognition of crop diseases through its recognition role and categorized expression of the results[22-24]. While it is possible to accurately recognize healthy crops from different types of diseased crops, it is rarely possible to accurately grade the expression of a particular disease on the basis of the damage caused by the crop disease. The impacts of climate change on crop diseases have been extensively studied worldwide. Various scientific studies have shown that the extent to which crops are exposed to diseases changes with the climate[25-27]. Thus image recognition alone is also unable to make accurate predictions of crop disease trends, especially over relatively short periods of time, such as a day to a week. And this part of the time is critical for disease prevention and control, because usually the pathogenic bacteria that harm crops grow very fast under suitable weather conditions and external environment.

The severity of crop disease prediction is an issue that must be clarified in order to guide the implementation of prevention and control strategies in production. Deep learning methods have produced research results in this area[28]. Tobacco weather fleck is a disease that is very closely related to climatic conditions, and it is only by understanding this relationship and screening for factors that have a significant correlation with disease incidence and trends that it will be possible to develop predictive systems that can reduce the growth of the disease. Generalized Additive Model (GAM) is used to model the relationship between the multiple response variable and predictor variables[29,30]. This approach not only screens the corresponding variables for a reasonable predictive model, but also helps to explain the effect of weather on tobacco weather spot disease, for which simple linear correlation is no longer sufficient.

In light of these challenges, the research focuses on Tobacco weather fleck. Firstly, we analyze the relationship between the weather data collected by the Internet of Things (IoT) devices and the occurrence of the disease, secondly, we employ the Long Short-Term Memory (LSTM) network and different optimization algorithms to build a prediction model of Tobacco weather fleck, and finally, we develop an image recognition model of Tobacco weather fleck with the help of image recognition technology using different models. We linked Tobacco weather fleck prediction model to an identification model. Rigorous model evaluation metrics were used to determine the accuracy and performance of the predictions. The schematic diagram of the study is shown in Fig. 1. This research provides modeling support for an IoT crop disease identification system that can help drive the deployment of (IoT) applications in agricultural practices.

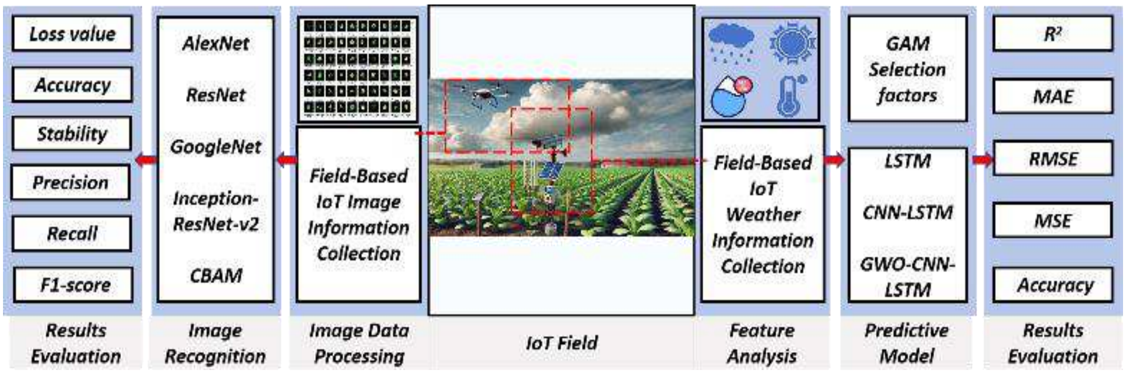

Fig. 1. Research schematic.

The main contributions of this article are as follows.

1) A Generalized Additive Model was used to fit the data in the IoT weather collection device to screen for factors that were significantly associated with different levels of Tobacco weather fleck.
2) Adopting and Improving Long Short-Term Memory for disease accurate grading prediction model.
3) Accurate identification of disease classification based on image recognition technology.

Materials and methods

Experimental design

The study was set in the tobacco-growing region of Chongqing, China (109°1′17″-109°45′58″E, 30°29′19″-31°22′33″N), which is located in the Yangtze River basin and within the Three Gorges Reservoir. The survey will be conducted from 2019-2024, from May through August each year. This period is the time when tobacco is growing in the field. Field control IoT collection equipment. The device can collect meteorological information such as temperature, humidity, light intensity and rainfall. The device also has a camera for taking field photos. Fig. 2 shows the experimental information and crop field growth. Tobacco weather fleck occurs in large fields due to climate change, the initial symptoms of the disease is the appearance of small white spots patches, followed by the spread of small white spots patches, during which sometimes brown spots appear, the onset of serious tobacco leaves on the main veins, lateral veins on both sides of the leaf tip, leaf surface will be intensively appeared spots, spots in the center of the necrosis of the collapse, the foliage tissue faded green[20]. According to the research description categorized normal and diseased tobacco into four grades[31,32], as shown in Fig. 3. Grade 0: normal tobacco with no disease infestation; Grade 1: a small number of spots on the leaf (Greater than 0% and less than or equal to 20%.); Grade 2: a large area of spots on the leaf (Greater than 20% and less than or equal to 50%.) with leaf damage; Grade 3: a large area of spots on the leaf (51% or more) with leaf breakage and wilting.

Fig. 2. Research base setup and IoT acquisition equipment.

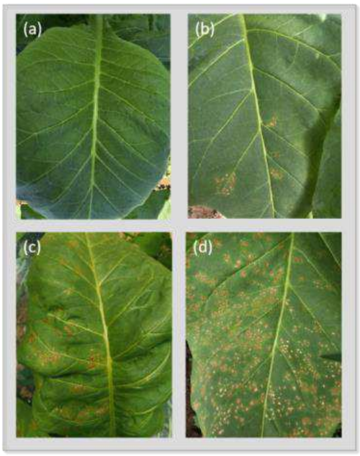

Fig. 3. Healthy leaves, grade 0 (Fig. 3a); lightly diseased leaves, grade 1 (Fig. 3b); moderately diseased leaves, grade 2 (Fig. 3c); and severely diseased leaves, grade 3 (Fig. 3d).

Disease significance factors

In Tobacco weather fleck prediction, predictions show a large correlation with climatic factors, but whether this relationship is linear or nonlinear has not been demonstrated. In the deep learning process, a large amount of data presenting very weak correlations is put into the training of algorithms, which often reduces the prediction accuracy and makes the prediction time too long. The reason is that the weakly correlated features have deep correlations with each other, and the redundant data input not only interferes with the training process, but also affects the stability of the model. Therefore, appropriate climate data features are selected for analysis. The generalized additive model is a nonlinear semiparametric regression model that examines the relationship between multiple independent variables and a dependent variable, allows to analyze both linear and nonlinear relationships. It is fitted using a nonlinear smoothing term that quantitatively explains the role of the independent variable in influencing the dependent variable[33]. Intrinsic functional form of the model:

$$g(E[y|X]) = \beta_0 + f_1(X_1) + f_2(X_2, X_3) + \cdots + f_M(X_N) \tag{1}$$

X_1, X_2, ... X_N are the independent variables; y is the dependent variable, *g ()* is the link function that relates the predictor variable to the expected value of the dependent variable; f_1, f_2, ... f_M are the characteristic functions applied to each predictor variable. In this study, different levels of tobacco climatic spot disease were used as response variables. in the model, and temperature, humidity, rainfall and light intensity collected by field IOT devices were used as explanatory variables in the model (Table 1). Variables with significant relationships in the model results were retained as inputs for disease prediction.

Serial Number	Parametric Item	IoT Data	Unit
1	X1	Daily maximum temperature	℃
2	X2	Daily minimum temperature	℃
3	X3	Dverage daily temperature	℃
4	X4	Duantity of daily rainfall	mm
5	X5	Average daily Relative Humidity	%RH
6	X6	Dverage daily light intensity	Lux

Table 1. Field iot collection equipment.

Disease prediction

Factors screened by the generalized additive model as having a significant effect on disease are categorized and used as inputs to the model. This study proposes three steps for disease prediction model construction. Given the property that the long short-term memory network (LSTM) model is able to learn the time series dependencies in the data by introducing a special structure and gating mechanism[34,35]. Firstly the long and short-term memory network model is selected for model construction. Further consideration is given to the fact that Convolutional Neural Networks (CNN) form a hierarchical structure through the stacking of multiple convolutional and pooling layers, which is capable of extracting features from simple to complex layer by layer, making the model capable of handling complex patterns[35]. Different types of climate parameters are used as inputs to the CNN layer, the features of the incoming parameters are extracted, and the corresponding feature vectors are built as inputs to the LSTM layer, and the CNN-LSTM model is built by optimizing the basic long and short-term memory network model through the above methods. Finally, the Gray Wolf Optimization (GWO) algorithm is used to optimize the values of the model parameters such as the number of neurons in the hidden layer and the learning rate of LSTM, and the model is optimized again to establish the GWO-CNN-LSTM model[36]. LSTM structure diagram, CNN framework diagram, and GWO optimization schematic are shown in Fig. 4. The flowchart of the model is shown in Fig. 5.

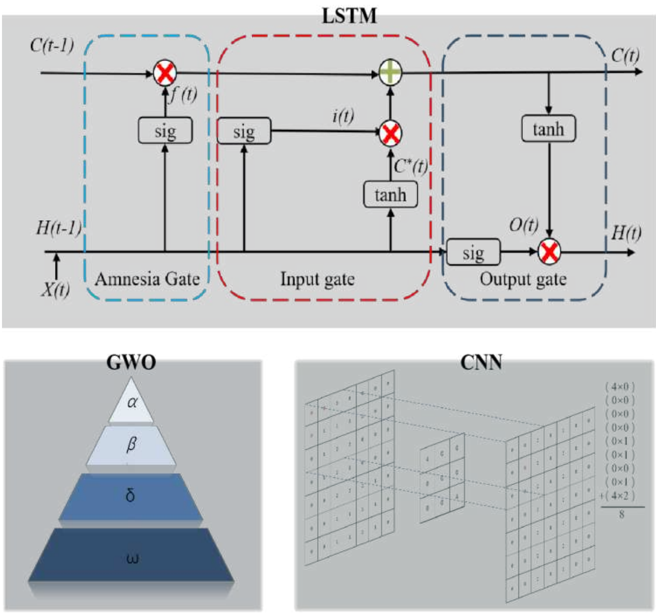

Fig. 4. LSTM structure; CNN convolutional layer schematic; Gray Wolf hierarchy.

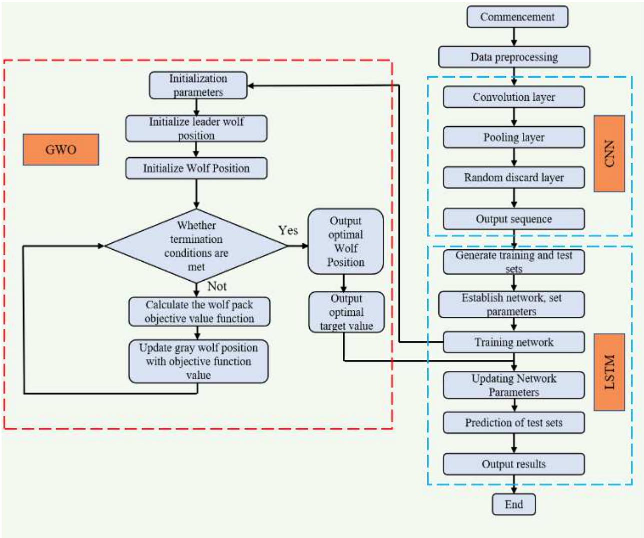

Fig. 5. Flowchart of the improved algorithm based on LSTM.

Distinct from the chained structure of the repetitive neural network module of an RNN, the forgetting gate *f(t)* is the first step in the work of the LSTM, which determines what is discarded from the previous cell state. The forgetting gate decides what to keep by reading the output *H(t - 1)* of the previous cell state and the current cell state input *x(t)*, which corresponds to the information *C(t - 1)* of the cell state at the previous moment through the *sig* function layer, in order to avoid the problem of gradient vanishing and explosion. The input gates *H(t - 1)* and *x(t)* are obtained through the *sig* function to the input gate *i(t)* to determine the values to be retained, through the *tanh* layer to the intermediate cell state information *C* (t)*, and update the cell state from *C(t - 1)* to the current cell state information *C(t)*. The output gate determines the output value based on the cell state, *H(t - 1)* and the output *O(t)* of the memory cell obtained from the *sig* function of *x(t)* to determine which part of the cell state needs to be output, and then multiply it with the value of *C(t)* obtained from the tanh layer, and the value is used as the output *H(t)*. The formula between each variable:

$$f(t) = sig\{W_f[H(t-1), x(t)] + b_f\} \tag{2}$$

$$i(t) = sig\{W_i[H(t-1), x(t)] + b_i\} \tag{3}$$

$$\mathrm{C^*(t) = tanh\{W_c[H(t-1), x(t)] + b_c\}} \tag{4}$$

$$\mathrm{C(t) = f(t)C(t-1) + i(t)C^*(t)} \tag{5}$$

$$\mathrm{O(t) = sig\{W_o[H(t-1), x(t)] + b_o\}} \tag{6}$$

$$\mathrm{H(t) = O(t)tanh[C(t)]} \tag{7}$$

In the equation: *Wf, Wi, Wc, Wo* are the weight matrices corresponding to each module in the forgetting gate, input gate, cell state update and output gate at time t, respectively; *bf, bi, bc, bo* are the bias terms of each module mentioned above.

Gray Wolf Optimization Algorithm A swarm intelligence algorithm that simulates the hierarchy and hunting behavior of gray wolves in nature through a four-layer structure. Layer 1: Alpha Tier Wolf Pack. Wolf pack leader - optimization algorithm optimal solution. Layer 2: *β*-layer wolves. Sub-leader of the wolf pack, assisting the wolves in the α-layer - suboptimal solution of the optimization algorithm. Layer 3: Layer δ wolves. Obey the decisions of α and β - poorly adapted α and β are downgraded to δ. Layer 4: ω-Level Wolves. Responsible for executing higher-level decisions and updating positions around α, β, and δ. As shown in Fig. 5. The algorithm optimization process is divided into three phases: encirclement, pursuit and attack. The formula is expressed as:

$$X(t-1) = X_p(t+1) - AD \quad (8)$$

$$D = \left|CX_p(t) - X(t)\right| \quad (9)$$

$$A = 2ar_1 - a \quad (10)$$

$$C = 2r_2 \quad (11)$$

X denotes the gray wolf position; it is the number of iterations; $X(t+1)$ denotes the gray wolf position after updating with the prey as the reference; X_P denotes the prey position; D is the distance vector between the gray wolf and the prey; r_1 and r_2 are random numbers in [0, 1]; A and C are the vector coefficients, and A denotes the simulated gray wolf's attack on the prey. Expressed as during the pursuit:

$$D_\alpha = |C_1 X_\alpha(t) - X(t)| \quad (12)$$

$$D_\beta = \left|C_2 X_\beta(t) - X(t)\right| \quad (13)$$

$$D_\delta = |C_3 X_\delta(t) - X(t)| \quad (14)$$

$$X_1 = X_\alpha(t) - A_1 D_\alpha \quad (15)$$

$$X_2 = X_\beta(t) - A_2 D_\beta \quad (16)$$

$$X_3 = X_\delta(t) - A_3 D_\delta \quad (17)$$

Equation: X_1, X_2 and X_3 are the distance vectors of ω from α, β and δ, respectively; $X(t+1)$ is the position of ω adjusted by α, β and δ. When the prey stops moving, the gray wolf completes the hunt by attacking. During the optimization process, when the value of a decreases linearly from 2 to 0, the value of A also varies in the interval [- a, a], and the wolves perform a global search when $A > 1$ and a local search when $A < 1$. The objective model optimization is completed by the above steps.

Disease identification

The objective is to achieve precise comprehension of the disease conditions through the deployment of field-based Internet of Things (IoT) devices. Consequently, machine learning methodologies are employed to accurately discern the severity levels of Tobacco weather fleck from image data. The widely used classical models AlexNet, ResNet101 and GoogLeNet are employed to train the Tobacco weather fleck data separately[37-39]. The optimal model is selected, based on which optimization and improvement are carried out to enhance the model performance. The structure of the three model networks is shown in Fig. 6.

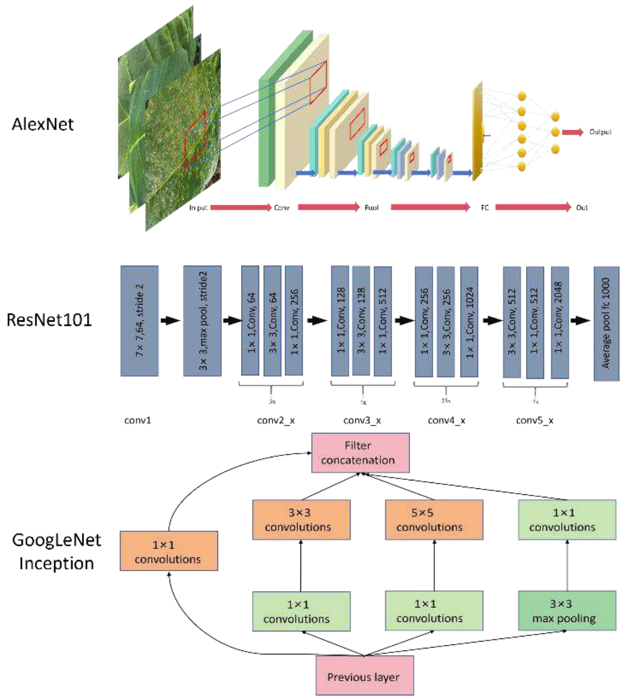

Fig. 6. Schematic of the three basic image recognition models.

The model with the highest accuracy and lowest loss value is selected among the three models for further improvement. The Inception-ResNet-v2 network, which combines the Inception module and the ResNet residual block, is used to improve model performance[40]. The main structure of the network consists of the stem network, the Inception-ResNet-A block, the Reduction-A dropout layer, the Inception-ResNet-B block, the Reduction-B dropout layer, the Inception-ResNet-C block, the global average pooling layer, the stopping of the overfitting layer (Dropout), the Softmax functions are constructed. The overall architecture is shown in Fig. 7.

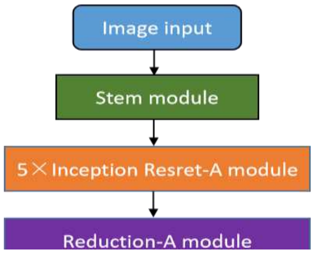

Fig. 7. General structure of the Inception-ResNet-v2 network.

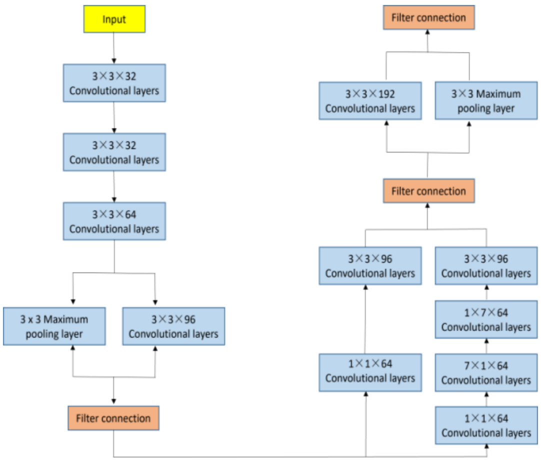

Fig. 8. Structure of stem.

The stem network included in Inception-ResNet-v2 is mainly used as a shallow feature extraction module. By combining many different types of convolutions in parallel, some of the structures split the large convolutional kernel into small convolutional kernels connected in series, and this asymmetric structure can be realized to extract structural features with more layers and increase the diversity. At the same time the maximum pooling layer and the convolutional layer are connected in parallel in the structure to avoid losing more data information by compressing the feature map too much (Fig. 8).

Fig. 9. Structure of Inception-ResNet-A; Inception-ResNet-B; Inception-ResNet-C.

There are three Inception-ResNet building blocks in the combinatorial network, and the three building blocks are the core part of the combinatorial network. The idea of connectivity of residual networks is added to the Inception module of multiplexed convolution, in which the structural blocks B and C have asymmetric convolutional structures (Fig. 9). The difference between the three blocks lies in the number of convolutional kernels, size and number of convolutional channels used in the Inception structure. The formulas for the three blocks are calculated as follows:

$$\begin{cases} h(x^{i+1}|\,\delta) = g\left(F\left(h(x^{i}|\,\delta)\right) + h(x^{i}|\,\delta)\right), \ \delta = A, B, C \\ L(l, n) = g\left(\sum_{j=1}^{m} L(l, j) * W_h^l + b_n^l\right) \end{cases} \tag{18}$$

where $h(x^i|\delta)$ denotes the structure block feature map of the ith Inception-ResNet- δ block ($\delta = A, B, C$), the function g denotes the network activation function, function F is the linear transformation function to compute the output features of the multiplexed convolution in the structured block, and $L(l,j)$ is labeled as the lth output in the lth layer of the convolutional network feature, W_h^l labeled as the nth weight parameter in the lth layer network, and b_n^l labeled as the nth weight parameter in the lth layer network. Classification performance degradation at the network structure level due to too deep layers is mitigated by different convolutional channels and asymmetric convolutional layers in the three modules.

The model was further optimized by adding the Convolutional Block Attention Module (CBAM), considering that the location of the affected leaves is often different in the same level of disease, which is not conducive to the accuracy after grading[41]. After passing through the Inception-ResNet-V2 network, the images of different disease levels first enter the channel attention module and then the spatial attention module. In the channel attention module, the input feature maps are compressed and aggregated based on the global maximum pooling layer and global average pooling layer to obtain two 1×1×C feature maps, and then they are fed into a 2-layer neural network (MLP) for summing operation. The specific structure is shown in Fig. 10.

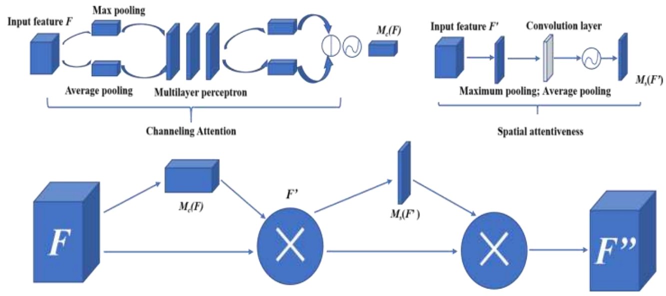

Fig. 10. CBAM attention mechanism structure.

CBAM includes two parts: channel attention mechanism and spatial attention mechanism. The calculation formula is as follows:

$$F' = M_c(F) \otimes F \tag{19}$$

$$F'' = M_s\left(F'\right) \otimes F' \tag{20}$$

In the formula: *F* denotes the input feature map; $\otimes$ is the multiplicative element; *F'* denotes the new feature obtained by channel attention as input to spatial attention; *F''* denotes the new feature obtained after spatial attention; M_C *(-)* denotes the one-dimensional channel attention generated after pooling; M_S *(-)* denotes the two-dimensional spatial attention generated after pooling. CBAM enhances the feature representation of diseased areas on tobacco leaves by emphasizing important feature channels through the channel attention mechanism and highlighting important spatial locations in the feature map through the spatial attention mechanism.

Evalution and verification

In the prediction model for Tobacco weather fleck, the model performance is evaluated using the following metrics: the coefficient of determination (R^2), mean absolute error (MAE), mean square error (MSE), Accuracy (Acc) and root mean square error (RMSE). For the Tobacco weather fleck disease grading recognition model, the performance is assessed using the F1 score, recall rate, precision, training set loss, test set loss, mean accuracy of the training set, mean accuracy of the test set.

Considering the practical application capabilities of the model, this study compares the accuracy of the Tobacco weather fleck disease model's predictive outcomes with the actual occurrence of diseases across different time periods. In this segment of the work, consideration is given to the timing of pesticide application and the scheduling of resources necessary for the control and prevention of tobacco climate spot diseases. The model under investigation is compared with the actual disease incidence to test the performance of prediction models in terms of accuracy when applied. To validate the accuracy of the Tobacco weather fleck disease grading identification model, we computed the discrepancies between the predictions made by the image recognition model and the actual outcomes. Additionally, we compared the accuracy of manual grading identification with that of the model's grading identification to assess the model's performance.

Experimental results

Data collection results

Between 2019 and 2024, a total of 3731 daily data entries were collected, comprising 3198 meteorological data points obtained through automated equipment and 533 records of disease incidence manually tabulated. Additionally, 2129 images of diseased plants were collected, categorized as follows: 250 images with no disease signs (level 0), 647 images with mild disease symptoms (level 1), 637 images with moderate symptoms (level 2), and 595 images with severe symptoms (level 3). The data were all collected during the growth period of tobacco in the field, including the rosette stage, vigorous growth stage, topping period, and initial harvest period.

Significance factor analysis

Utilizing the gamm function from the mgcv package in R software to fit the generalized additive model for significant factors of Tobacco weather fleck disease. The generalized additive model is composed of a parametric component with an intercept and a non-parametric component with smoothing terms. The fitting results are presented in Table 2. It can be observed that the variables affecting the fitting results include Daily minimum temperature, Average daily temperature, Quantity of daily rainfall, Average daily relative humidity, and Average daily light intensity. Upon conducting a significance test for the non-parametric terms of each model, P-values were found to be less than 0.05, indicating that these variables have a significant impact on the occurrence of Tobacco weather fleck disease.

Parametric term					Nonparametric term		
Intercept	Estimated value	SE	t value	P value	Smooth term	F value	P value
α1	0.35	0.01	29.04	<0.05	X1	1.19	0.38
					X2	5.02	<0.05
					X3	3.42	<0.05
					X4	2.86	<0.05
					X5	9.04	<0.05
					X6	2.46	<0.05

Note: α1 denotes the corresponding intercept of the model.

Table 2. Results of generalized additive model for significant factor analysis of tobacco weather fleck disease.

Based on the partial residual distribution plot (Fig. 11) from the analysis of significant factors for Tobacco weather fleck disease, it is evident that the residual plots for parameter terms X1, X2, X3, X5, and X6 are uniformly distributed, while the residual plot for parameter term X4 is concentrated in the range of 0-0.25. This suggests that there is a significant nonlinear relationship between the quantity of daily rainfall and the occurrence of tobacco climate spot disease. The parameter term X1 did not meet the criterion of P < 0.05, indicating that there is no significant relationship between daily maximum temperature and the incidence of Tobacco weather fleck disease.

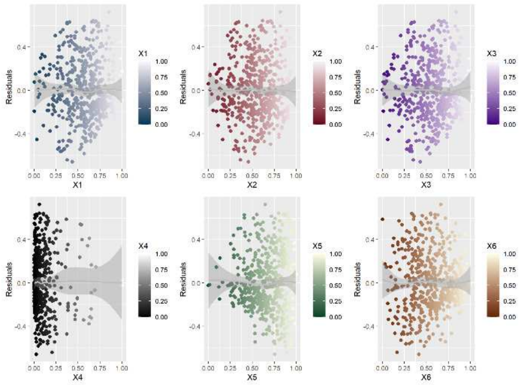

Fig. 11. Partial residuals of components for generalized additive models.

Results of the lSTM-model based

The features with significant influence on the incidence of Tobacco weather fleck disease were screened as the entry factors of the tobacco climacteric spot disease prediction model, and the output was the prediction result of the disease condition. An LSTM (Long Short-Term Memory) model is employed for data fitting. The distribution plot of actual versus predicted values within the test set (Figure 12), in conjunction with the model parameter values (Table 3), poor reliability of model predictions for Tobacco weather fleck disease classification.

Model/ Parametric	Acc	R^2	RMSE	MSE	MAE
LSTM	0.79	0.46	0.74	0.93	0.61
CNN-LSTM	0.81	0.59	0.51	0.41	0.47
GWO-CNN-LSTM	0.89	0.68	0.45	0.24	0.31

Table 3. Parameters of three training models for disease prediction.

Fig. 12. Distribution of predicted and actual values for the validation set of the LSTM model.

Based on imprroved LSTM model results

Input data significantly correlated with the incidence of Tobacco weather fleck disease into a Convolutional Neural Network (CNN) for feature extraction to further optimize the Long Short-Term Memory (LSTM) model. Subsequently, integrate the Grey Wolf Optimizer (GWO) trained network with the CNN-LSTM model to enhance its predictive performance. The model fitting results indicate (Fig. 13) that the GWO-CNN-LSTM model demonstrates a closer predictive performance to the actual occurrence of tobacco climate spot disease in the test set compared to the CNN-LSTM model. An analysis of the fitting residuals of the three predicted results, CNN-LSTM, and GWO-CNN-LSTM models and the actual values reveals that the LSTM model's fitting residuals show a significant difference from the other two models and have a higher mean, indicating that its stability in fitting Tobacco weather fleck disease is inferior to that of the two optimized models.

The performance results of the two optimized models indicate (Table 3) that the GWO-CNN-LSTM model has a higher R^2 value and lower Mean Absolute Error (MAE), MSE and Root Mean Square Error (RMSE) values compared to the CNN-LSTM model. The GWO-CNN-LSTM model has the highest accuracy, followed by CNN-LSTM, and the LSTM model has the lowest accuracy. This suggests that the optimization effect of the Grey Wolf Algorithm on the Convolutional Neural Network combined with the Long Short-Term Memory model is more suitable for serving as a predictive model for Tobacco weather fleck disease.

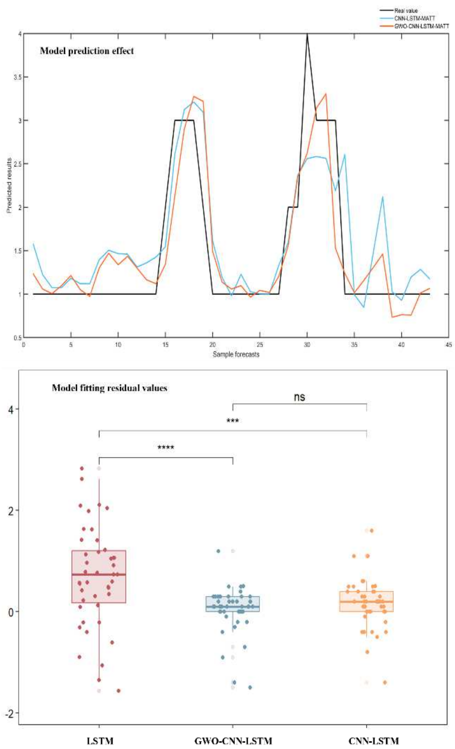

Fig. 13. CNN-LSTM model and GWO-CNN-LSTM model of Tobacco weather fleck disease test set prediction and true value fitting results.

Tobacco disease image enhancement results

To enhance the generalization capability of the Tobacco weather fleck disease grading recognition model and to mitigate the instability caused by overfitting, data augmentation techniques were applied to the collected disease images. The results of image data augmentation include (Fig. 14): randomly rotating images with angles ranging from -45 degrees to 45 degrees; cropping a 224x224 pixel region from the center of the image; horizontally flipping the image with a probability of 50%; vertically flipping the image.

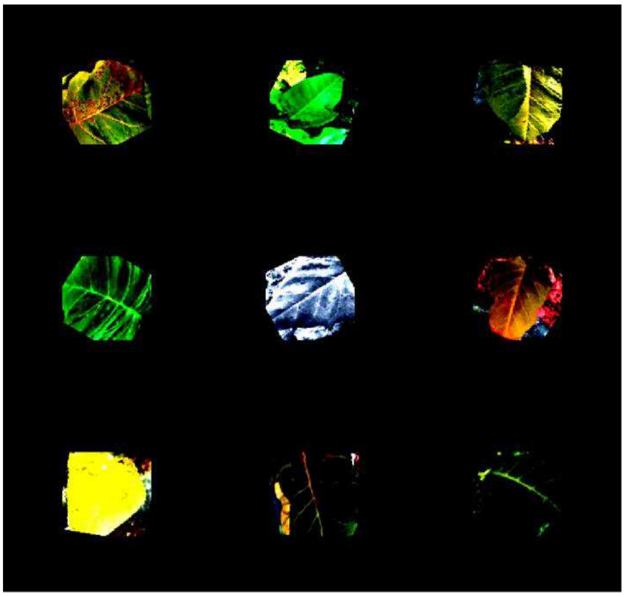

Fig. 14. Effects of image data enhancement for Tobacco weather fleck disease.

Disease classification identification results

In this experiment, three representative convolutional neural network structures, AlexNet, ResNet101, and GoogleNet, were selected. Transfer learning was performed using the Adam optimizer for each network, and the original loss function was further optimized. The accuracy and loss values of the established Tobacco weather fleck disease grading recognition model are shown in Fig. 15 and Table 4.

Model/Parametric	Average training loss	Average training accuracy	Average testing loss	Average testing accuracy	Precision	Recall	F1-score
ResNet-101	0.56	0.79	1.09	0.61	0.68	0.62	0.65
AlexNet	1.19	0.66	1.23	0.53	0.56	0.52	0.54
GoogleNet	0.52	0.79	0.41	0.85	0.89	0.86	0.87

Table 4. Average parameters of three training models for image recognition.

The loss rate of the model training set gradually decreased with the number of iterations and stabilized after the 5th iteration. The ResNet-101 and GoogleNet models exhibited overall lower loss values compared to the AlexNet model, with the GoogleNet model demonstrating the most stable loss curve (Fig. 15a). The loss values on the test set fluctuated more significantly compared to the training set, but the overall loss rate also showed a gradual decrease with increasing iterations, with the GoogleNet model's test set loss curve being significantly lower than the other two models (Fig. 15b). The accuracy rate on the training set stabilized after 5 iterations, with the AlexNet model's accuracy fluctuating around 0.65, and the ResNet-101 and GoogleNet models' accuracies fluctuating around 0.8, although the ResNet-101 model showed a slightly higher overall accuracy rate in the later stages of training (Fig. 15c). The accuracy rate on the test set fluctuated more significantly compared to the training set, with the GoogleNet model's accuracy rate being significantly higher than the other two models (Fig. 15d). The model parameters are detailed in Table 3, where the GoogleNet model showed good performance in terms of average loss, average accuracy, Precision, Recall, and F1-score. A comprehensive analysis indicates that the GoogleNet model outperforms the ResNet-101 and AlexNet models in the classification and recognition of Tobacco weather fleck disease.

Fig. 15. Variation of alias accuracy and loss values with the number of iterations for different models.

Googlenet optimization algorithm results

To further enhance the accuracy of the tobacco climate spot disease grading recognition model, the GoogleNet model was selected and improved upon. The Inception-ResNet-v2 structural network was introduced as the feature extraction framework for identification training. Furthermore, a CBAM (Convolutional Block Attention Module) lightweight attention module was added to the output layer of the improved model to enhance the model's classification attention recognition. After 100 iterations, the results are shown in Fig. 16. The loss curve and accuracy curve indicate that both improvements based on the GoogleNet model are superior to the base model. The analysis of model parameters (Table 5) shows that the introduction of the Inception-ResNet-v2 structure significantly increased the accuracy of disease grading recognition. Although the training set loss value of the

CBAM-Inception-ResNet-v2-GoogleNet model established after adding the CBAM module slightly exceeds that of the Inception-ResNet-v2-GoogleNet (0.0004), the test set loss value is relatively lower. Moreover, this model has a higher training set accuracy and test set accuracy, as well as more stable curve output. Therefore, the CBAM-Inception-ResNet-v2-GoogleNet model is more suitable for tobacco climate spot disease grading recognition.

Fig. 16. Variation of Recognition Accuracy and Loss Values with Number of Iterations for Two Modified GoogleNet-Based Models and GoogleNet Model.

Model/Parametric	Average training loss	Average training accuracy	Average testing loss	Average testing accuracy	Precision	Recall	F1-score
CBAM-Inception-ResNet-v2	0.1196	0.9582	0.1028	0.9665	0.9764	0.9752	0.9758
GoogleNet	0.5244	0.7976	0.4101	0.8461	0.8909	0.8662	0.8783
Inception-ResNet-v2	0.1192	0.9579	0.1074	0.9640	0.9397	0.9106	0.9249

Table 5. Average parameters of two improved model image recognition training models.

Model validation

In consideration of the control and application of pesticides for tobacco climate spot disease, a grading prediction model for tobacco climate spot disease was established to forecast the disease status from the current day to five days ahead, totaling six days. The results indicate (Fig. 17a): there is no significant difference in the average accuracy between the predictions for the first two days and the first four days. However, a significant difference in accuracy is observed from the fifth day onwards, with a substantial decrease in accuracy. This suggests that the tobacco climate spot prediction model is suitable for disease grading prediction within four days; beyond four days, the accuracy significantly declines.

The validation results of the tobacco climate spot disease grading recognition model are presented in Fig. 17b. The model's accuracy in disease identification is significantly higher than that of manual identification. Across different levels of disease severity, the results derived from the model are consistently higher than those obtained from human experience (Table 6). This indicates that the tobacco climate spot disease grading recognition model possesses excellent recognition capabilities.

Fig. 17. Validation of a hierarchical prediction model for tobacco climacteric spot disease.

Model/Manual	Level 0	Level 1	Level 2	Level 3
Model identification	0.9066	0.8951	0.8989	0.9153
Artificial identification	0.8956	0.8852	0.6751	0.8602

Table 6. Identification of different levels of disease.

Discussion

A literature review conducted in this study confirmed that tobacco climate spot disease is a non-infectious type of lesion[20,21]. This determination is of paramount importance, as it influences whether Internet of Things (IoT) devices must capture pathogen spore data as an essential indicator for the prediction of disease severity grading[42]. The use of field-based Internet of Things (IoT) devices to collect meteorological data for the establishment of a tobacco climate spot disease prediction model, rather than directly employing images for prediction, is grounded in the literature review that elucidates climate as a primary factor in the occurrence of the disease. However, previous scientific research has only provided empirical descriptions of different disease scenarios without offering precise grading expressions for the severity of the disease's occurrence. Crop disease grading is crucial for the deployment of control strategies, such as the type of pesticide to be applied, the dosage, and the timing of application. Our approach is to leverage field-based Internet of Things (IoT) devices to achieve precise identification of tobacco climate spot disease severity (utilizing image recognition technology) and accurate forecasting of disease occurrence (modeling based on meteorological data).

Selecting appropriate meteorological data for the construction of a disease prediction model involves initially identifying factors that have a significant correlation with the occurrence of the disease. This not only aids in elucidating the patterns of disease development but also alleviates the data processing burden on IoT devices. Based on the existing research findings, we cannot assume a linear or nonlinear relationship between the factors associated with the occurrence of the disease. Generalized Additive

Models (GAMs), which combine the advantages of linear models and non-parametric models, have been widely applied in various fields to study complex dependency relationships[43-45]. In this study, we have not analyzed the interactive effects among multiple factors, as the climate in open-field agricultural production is inherently complex and variable, a condition that is particularly prevalent in mountainous regions[46,47]. After identifying the factors significantly associated with the occurrence of tobacco climate spot disease, various machine learning methods (basic models) were employed to construct the predictive models. The model with the optimal performance was selected for further optimization to enhance its predictive accuracy and applicability.

Among the three classic image recognition models selected, GoogleNet demonstrated excellent performance in disease grading identification. In further optimizing the recognition model, we considered improvements in both the deep learning network architecture and the attention mechanism modules. The advantages brought about by such enhancements have been widely validated[48,49]. The findings of this study also confirm that the incorporation of the Inception-ResNet-v2 architecture with the Convolutional Block Attention Module (CBAM) can lead to reduced loss values and increased accuracy in the tobacco climate spot disease grading recognition model.

Conclusion

This study employs IoT-based meteorological data collection to construct a GWO-CNN-LSTM model for the grading prediction of tobacco climate spot diseases, achieving an average accuracy of 85.46% over a four-day period. It has been established that Daily Minimum Temperature (DMT), Average Daily Temperature (ADT), Quantity of Daily Rainfall (QDR), Average Daily Relative Humidity (ADRH), and Average Daily Light Intensity (ADLI) are significantly correlated with the occurrence of diseases. Furthermore, a CBAM-Inception-ResNet-v2-GoogleNet model was developed to achieve a grading recognition accuracy of 92.40%, surpassing manual grading accuracy. The research outcomes provide model support for the automatic recognition of field diseases and the deployment of IoT, offering case support for the application of smart agriculture IoT. In this study, further research on multiple tobacco varieties and the ecological patterns of farmland landscapes was not conducted, which may have potential implications for the application. Future work should consider further improvements in this area.

Data availability

The datasets used and/or analyzed during the current study available from the corresponding author W. D. or first author J.S. on reasonable request.

References

1. Keating, B. A., Herrero, M., Carberry, P. S., Gardner, J. & Cole, M. B. Food wedges: Framing the global food demand and supply challenge towards 2050. *Glob. Food Secur.* **3**, 125–132 (2014).
2. Lioutas, E. D., Charatsari, C., & De Rosa, M. Digitalization of agriculture: A way to solve the food problem or a trolley dilemma? *Technol. Soc.* **67**, 101744 (2021).
3. Misra, N. N. et al. IoT, big Data, and artificial intelligence in agriculture and food industry. *IEEE Internet Things J.* **9**(9), 6305–6324 (2022).
4. Xue, D. & Huang, W. Smart agriculture wireless sensor routing protocol and node location algorithm based on internet of things technology. *IEEE Sens. J.* **21**(22), 24967–24973 (2021).
5. Boursianis, A. D. et al. Internet of Things (IoT) and Agricultural Unmanned Aerial Vehicles (UAVs) in smart farming: A comprehensive review. *Internet Things (Amst.)* **18**, 100187 (2022).
6. Worrall, E. A., Hamid, A., Mody, K. T., Mitter, N. & Pappu, H. R. Nanotechnology for plant disease management. *Agronomy* **8**(12), 285 (2018).
7. Carvajal-Yepes, M. et al. A global surveillance system for crop diseases. *Science* **364**(6447), 1237–1239 (2019).
8. Saggi, M. K. & Jain, S. A survey towards decision support system on smart irrigation scheduling using machine learning approaches. *Arch. Comput. Methods Eng.* **29**(6), 4455–4478 (2022).
9. Tito, R. H., Vasconcelos, L. & Feeley, K. J. Global climate change increases risk of crop yield losses and food insecurity in the Tropical Andes. *Glob. Change Biol.* **24**(2), E592–E602 (2018).
10. Liu, Z. et al. Internet of Things (IoT) and machine learning model of plant disease prediction–blister blight for tea plant. *IEEE Access* **10**, 44934-44944 (2022).
11. Singh, M., Savary, S., Setiya, P., Tewari, A. K. & Nain, A. S. Multivariate analysis of the effects of weather variables on white rust epidemics and yield reduction of mustard over multiple growing seasons. *Plant Pathol.* **73**(4), 791–809 (2024).
12. Lu, J., Wu, Z., Lan, Y., Deng, X. & Huang, J. Study on the prediction model of litchi downy blight damage based on IoT and hyperspectral data fusion. *IEEE Internet Things J.* **11**(16), 27184–27200 (2024).
13. Kim, Y., Roh, J. H. & Kim, H. Y. Early forecasting of rice blast disease using long short-term memory recurrent neural networks. *Sustainability* **10**(1), 34 (2018).
14. Krishna R. & Prema, K. V. Constructing and optimizing RNN models to predict fruit rot disease incidence in areca nut crop based on weather parameters. *IEEE Access* **11**, 110582-110595 (2023).
15. Lara-Benítez, P., Carranza-García, M. & Riquelme, J. C. An experimental review on deep learning architectures for time series forecasting. *Int. J. Neural Syst.* **31**(3), 2130001 (2021).
16. Rostamian A. & O'Hara, J. G. Event prediction within directional change framework using a CNN-LSTM model. *Neural Comput. Appl.* **34**(20), 17193–17205 (2022).
17. Van Houdt, G., Mosquera, C. & Nápoles, G. A review on the long short-term memory model. *Artif. Intell. Rev.* **53**(8), 5929–5955 (2020).
18. Lencucha, R. et al. The political economy of tobacco in Mozambique and Zimbabwe: A triangulation mixed methods protocol. *Int. J. Environ. Res. Public Health* **17**(12), 4262 (2020).

19. Nguenha, N., Cunguara, B., Bialous, S., Drope, J. & Lencucha, R. An overview of the policy and market landscape of tobacco production and control in Mozambique. *Int. J. Environ. Res. Public Health* **18**(1), 343 (2021). .

20. Heggestad, H. E. & Middleton, J. T. Ozone in high concentrations as cause of tobacco leaf injury. *Science* **129**(3343), 208–210 (1959).

21. Macdowall, F. D. H. Predisposition of tobacco to ozone damage. *Can. J. Plant Sci.* **45**(1), 1–12 (1965).

22. Haridasan, A., Thomas, J. & Raj, E. D. Deep learning system for paddy plant disease detection and classification. *Environ. Monit. Assess* **195**(1), 120 (2023). .

23. Lu, Y., Yi, S., Zeng, N., Liu, Y. & Zhang, Y. Identification of rice diseases using deep convolutional neural networks. *Neurocomputing* **267**, 378-384 (2017).

24. Ma, J. et al. A recognition method for cucumber diseases using leaf symptom images based on deep convolutional neural network. *Comput. Electron. Agr.* **154**, 18-24 (2018).

25. Dentika, P., Ozier-Lafontaine, H. & Penet, L. Dynamics of pathogenic fungi in field hedges: Vegetation cover is differentially impacted by weather. *Microorganisms* **10**(2), 400 (2022).

26. Madgwick, J. W. et al. Impacts of climate change on wheat anthesis and fusarium ear blight in the UK. *Eur. J. Plant Pathol.* **130**(1), 117–131 (2011).

27. Pfordt, A. L., Romero, R., Schiwek, S., Karlovsky, P. & von Tiedemann, A. Impact of environmental conditions and agronomic practices on the prevalence of *Fusarium* species associated with ear- and stalk rot in maize. *Pathogens* **9**(3), 236 (2020).

28. Kundu, N. et al. Disease detection, severity prediction, and crop loss estimation in MaizeCrop using deep learning. *Artif. Intell. Agric.* **6**(1), 276-291 (2022).

29. Aghajanlou, F. et al. Rangeland management and ecological adaptation analysis model for astragalus curvirostris boiss. *Horticulturae* **7**(4), 67 (2021).

30. Feng, Y. & Tong, X. Calibrating nonparametric cellular automata with a generalized additive model to simulate dynamic urban growth. *Environ. Earth Sci.* **76**(14), 496 (2017).

31. Huang, L. et al. Causal factors of the weather fleck of tobacco. *Acta Phytop Sin.* **25**(3), 285-288 (1995).

32. Cheng, J., Xiong, K. & Wang, Y. Tobacco Weather Fleck Disease. *Acta Tab Sin*. **4**(1), 54-59 (1998).

33. Pedersen, E. J., Miller, D. L., Simpson, G. L. & Ross, N. Hierarchical generalized additive models in ecology: An introduction with mgcv. *PeerJ.* **7**(3), e6876 (2019).

34. Sangeetha S, et A multi-modal geospatial-temporal LSTM based deep learning framework for predictive modeling of urban mobility patterns. *SCI REP-UK* **14,** 31579 (2024).

35. Gu, J. et al. Recent advances in convolutional neural networks. *Pattern Recogn.* **77**, 354-377 (2018).

36. Makhadmeh, S. N. et al. Recent advances in Grey Wolf optimizer, its versions and applications: Review. *IEEE Access* **12**, 22991-23028 (2024).

37. Kolhar M & Al Rajeh AM. Deep learning hybrid model ECG classification using AlexNet and parallel dual branch fusion network model. *SCI REP-UK* **14**, 26919 (2024).

38. Huang, M. & Xu, Y. Image classification of Chinese medicinal flowers based on convolutional neural network. *Math. Biosci. Eng.* **20**(8), 14978–14994 (2023).

39. Yang, L. et al. GoogLeNet based on residual network and attention mechanism identification of rice leaf diseases. *Comput. Electron. Agr.* **204**, 107543 (2023).

40. Wang, J. et al. A real-time bridge crack detection method based on an improved Inception-Resnet-v2 structure. *IEEE Access* **9**, 93209-93223 (2021).

41. Wang, W., Tan, X., Zhang, P. & Wang, X. A CBAM based multiscale transformer fusion approach for remote sensing image change detection. *IEEE J. Sel. Top. Appl. Earth Obs. Remote Sens.* **15**, 6817-6825 (2022).

42. Singh B. K. et al. Climate change impacts on plant pathogens, food security and paths forward. *Nat. Rev. Microbiol.* **21**(10), 640–656 (2023).

43. Cai, L. R. et al. Global models and predictions of plant diversity based on advanced machine learning techniques. *New Phytol.* **237**(4), 1432–1445 (2023).

44. Dodangeh, E. et al. Integrated machine learning methods with resampling algorithms for flood susceptibility prediction. *Sci. Total Environ.* **705**, 135983 (2020).

45. Zhao, W., Zhao, L., Chang, X., Lu, X. & Tu, Y. Elevated dementia risk, cognitive decline, and hippocampal atrophy in multisite chronic pain. *Proc. Natl. Acad. Sci. USA.* **120**(9), e2215192120 (2023).

46. Quintero, I., Jetz, W. Global elevational diversity and diversification of birds. *Nature* **555**, 246–250 (2018).

47. Carsten Rahbek et al. Humboldt's enigma: What causes global patterns of mountain biodiversity?. *Science* **365**, 1108-1113 (2019).

48. Al-masni, M. A., Kim, D. H. & Kim, T. S. Multiple skin lesions diagnostics via integrated deep convolutional networks for segmentation and classification. *Comput. Meth. Prog. Bio.* **190**, 105351 (2020).

49. Chen, S. et al. Remote sensing scene classification via multi-branch local attention network. *IEEE Trans. Image Process.* **31**, 99-109 (2022).

Acknowledgements

This research was financially supported by the Construction of digital model of production technology based on tobacco quality assurance under Grant 0633-224042118J00.

Author contributions

Conceptualization, J.S., X.H.; methodology, J.S., Y.R.; software, J.S;. validation, Z.W., Y.J.; investigation, J.S., X.H.; resources, G.M.; supervision, W.D.

Competing interests

The authors declare no competing interests.